Mechanical Systems and Signal Processing 96 (2017) 139–158

Contents lists available at ScienceDirect

Mechanical Systems and Signal Processing

journal homepage: www.elsevier.com/locate/ymssp

Excitation power quantities in phase resonance testing of nonlinear systems with phase-locked-loop excitation

Simon Peter *, Remco I. Leine

Institute for Nonlinear Mechanics, University of Stuttgart, Pfaffenwaldring 9, 70569 Stuttgart, Germany

ARTICLE INFO

Article history:
Received 10 June 2016
Received in revised form 7 April 2017
Accepted 9 April 2017

Keywords:
Nonlinear normal modes
Phase resonance testing
Nonlinear mode indicator function
Phase-locked-loop
Nonlinear system identification

ABSTRACT

Phase resonance testing is one method for the experimental extraction of nonlinear normal modes. This paper proposes a novel method for nonlinear phase resonance testing. Firstly, the issue of appropriate excitation is approached on the basis of excitation power considerations. Therefore, power quantities known from nonlinear systems theory in electrical engineering are transferred to nonlinear structural dynamics applications. A new power-based nonlinear mode indicator function is derived, which is generally applicable, reliable and easy to implement in experiments. Secondly, the tuning of the excitation phase is automated by the use of a Phase-Locked-Loop controller. This method provides a very user-friendly and fast way for obtaining the backbone curve. Furthermore, the method allows to exploit specific advantages of phase control such as the robustness for lightly damped systems and the stabilization of unstable branches of the frequency response. The reduced tuning time for the excitation makes the commonly used free-decay measurements for the extraction of backbone curves unnecessary. Instead, steady-state measurements for every point of the curve are obtained. In conjunction with the new mode indicator function, the correlation of every measured point with the associated nonlinear normal mode of the underlying conservative system can be evaluated. Moreover, it is shown that the analysis of the excitation power helps to locate sources of inaccuracies in the force appropriation process. The method is illustrated by a numerical example and its functionality in experiments is demonstrated on a benchmark beam structure.

1. Introduction

Experimental modal analysis (EMA) is the most common procedure for the identification of linear dynamic structures. It provides a very user-friendly way of extracting comprehensive information about the dynamic properties of a system. However, its limitation to linear systems has become more and more substantial as the complexity of engineering structures grows and the demand for light-weight and efficient structures increases. Many of these requirements cannot be met without explicitly taking into account nonlinearity in the design process. This development poses new challenges for the numerical and the experimental analysis in structural dynamics.

On the experimental side this generates a need for reliable and easy to use nonlinear system identification techniques. Even though there are numerous techniques for nonlinear identification [1,2] many of them are limited to small scale systems, weak nonlinearity or are difficult to relate to a clear physical meaning [3]. Oftentimes, it is also required to investigate the linear structure separately from the nonlinearities which requires additional experimental effort.

* Corresponding author.
E-mail addresses: peter@inm.uni-stuttgart.de (S. Peter), leine@inm.uni-stuttgart.de (R.I. Leine).

http://dx.doi.org/10.1016/j.ymssp.2017.04.011
0888-3270/

A promising concept to overcome some of these drawbacks is the concept of nonlinear modes, which provides global information about the system's linear and nonlinear dynamics along with a clear physical meaning [4]. The concept was introduced in the 1960s by Rosenberg as an extension of linear normal modes (LNM) to nonlinear systems [5]. A nonlinear normal mode (NNM) according to Rosenberg's definition is a synchronous, periodic motion of a conservative system. This definition provides a clear theoretical framework and a direct relation to linear modes. An extension of the concept of nonlinear modes to non-conservative systems was provided by Shaw and Pierre in the 1990s [6] who showed that the nonlinear modal motion can be regarded as a motion on an invariant manifold in the phase space. Despite the generality of this definition and its valuable theoretical insights to nonlinear modal dynamics most practical applications still basically rely on Rosenberg's definition. This is partly due to the fact that there are powerful and reliable numerical algorithms like the shooting method [7] or the Harmonic Balance Method (HBM) [8] for the calculation of the periodic motions on a NNM branch. Moreover, nonlinear modal interactions can be resolved in a straightforward way by extending Rosenberg's definition to non-necessarily synchronous periodic motions as it has been done by Kerschen [4].

Generally, the modes of the underlying undamped system provide valuable insight into the dynamics of the damped system and the assessment of the undamped modes is therefore for linear systems common practice [9]. The first approach for nonlinear EMA, presented by Peeters [10], extended phase resonance testing to nonlinear structures, and also essentially relies on the definitions of Rosenberg and Kerschen for conservative nonlinear modes. More recent phase separation methods for nonlinear modal analysis [11] are based on the same framework. The efficient numerical algorithms for the calculation of NNMs furthermore provide a powerful tool for parameter estimation based on experimental data [12]. In this paper NNMs are defined according to Rosenberg's definition with the extension of Kerschen, such that internal resonances are generally taken into account, even though they are not the main focus of this work.

The phase resonance method, which was proposed by Peeters in 2010 [10] and subsequently proved its applicability in several experimental studies [10,13,14], poses some practical difficulties. In this approach the excitation frequency of a forced and damped system is varied manually until the NNM motion of the underlying conservative system is approximately isolated. This is a difficult and very time consuming procedure. Especially lightly damped systems, which are indeed the systems of interest in an NNM analysis, are very sensitive to changes of the excitation frequency near sharp resonance peaks of the frequency response. The increments of the excitation frequency have therefore to be very small near resonance in order to isolate an NNM motion. Furthermore, in the case of strong nonlinearities where a jump occurs in the frequency response function (FRF) in the vicinity of the resonance even small perturbations lead to a premature jump and require the experimentalist to start the elaborate tuning process all over again. Due to this extensive effort for the appropriation of a single NNM typically the invariance property of the invariant manifold of the associated free and damped system is exploited to extract the remaining NNMs of the same branch: Once the NNM is isolated by an appropriate force, the excitation is switched off and it is assumed that the motion of the damped system decays on the invariant manifold of the free and damped system. For light damping the motion of the free and damped system closely resembles the motion of the free and undamped system, i.e. the NNM motion. Due to the dissipation the vibration energy decreases successively such that an approximate NNM motion for different energy levels can be obtained. To extract the frequency-energy dependence of the NNM, a time frequency analysis is carried out on the recorded free-decay data. This requires sophisticated signal processing such as wavelet transform (WT) [15], Hilbert transform [16] or short time Fourier transform [17] and the degree of damping limits the resolution of the recorded backbone curve. The influence of transient effects is not clear for all systems, particularly when the excitation system, e.g. the shaker, remains connected to the structure during free-decay measurement. Moreover, there exists no method for the evaluation of the quality of the NNMs obtained by analyzing the free-decay data.

This paper presents a new approach for phase resonance testing to overcome the practical issues of the previous method. Therefore, the objective of the paper is twofold: Firstly, criteria for the evaluation of the NNM quality are derived and secondly a user-friendly way of force appropriation is presented. For the evaluation of the NNM quality a series of steady-state measurements for varying excitation levels is used instead of the free-decay measurements that are used in traditional phase resonance testing. The time consuming tuning of the excitation frequency has therefore to be simplified in order to obtain results within reasonable time. Thereto, a Phase-Locked-Loop (PLL) controller is implemented. The PLL is used for maintaining the phase lag quadrature criterion for the fundamental harmonic of the excitation. The desired phase of the excitation is reached automatically and very fast by the closed loop control. The frequency of excitation is inherently obtained by the structure's response. Thus, additional benefits of phase control like its robustness in lightly damped systems and the possibility of stabilization of unstable branches can be exploited. By the use of steady-state measurements transient effects are eliminated and the resolution of the measured backbone curve can be chosen arbitrarily. Furthermore, the steady-state tests with a known excitation force make it possible to evaluate the quality of the NNM appropriation for every point on the backbone curve.

When an approximate fundamental harmonic forcing is used for the excitation of the structure it is not sufficient to solely consider the phase of the fundamental harmonic as a quality indicator for the NNM isolation, as higher harmonics may be present in the forced response as well as in the NNM motion. Therefore, Peeters proposed a response based modal purity index (MPI) [10], which basically considers the phase of the fundamental and higher harmonics of the response. This MPI is restricted to monophase motions and theoretically has to be evaluated for all points on the structure simultaneously, which requires high experimental effort. Moreover, the result is highly dependent on the number of harmonics considered [18]. In contrast, in this paper a novel, excitation power based mode indicator function (PBMIF) will be presented which is simpler to implement experimentally, more reliable and general. The central quantity which has to be considered to calculate this PBMIF is the mechanical power of the excitation. In order to assess the characteristics of the excitation power in context with a nonlinear phase resonance test, power quantities known from nonlinear electrical systems are transferred to nonlinear mechanical systems. The power of the excitation can be easily obtained in experiments by measuring only the force and the response at the excitation point. The new PBMIF is independent of the number of harmonics considered and also valid for situations where there is a phase difference between different harmonics. In addition to the global indication of the NNM appropriation quality with the PBMIF, the analysis of the excitation power components also offers practical indications how to improve the force appropriation quality.

The paper is organized as follows. In Section 2 the methodology of phase resonance testing is briefly reviewed and a pointer notation for the dynamic forces in the frequency domain is introduced. This pointer notation is then used in Section 3 to explain the role of the excitation power in nonlinear modal testing and derive a power based mode indicator function. Subsequently, in Section 4 the control concept of the PLL is briefly explained and the specific implementation used for nonlinear phase resonance testing is discussed. The application of the PLL and the tuning of the PLL parameters for phase resonance testing is illustrated on the basis of a numerical example in Section 5. In Section 6, the method is applied experimentally to a benchmark beam structure featuring a cubic nonlinearity. The paper concludes with Section 7.

2. Phase resonance testing

The phase resonance method, in the linear as well as in the nonlinear case, aims at exciting a damped structure such that the normal mode motion of the underlying conservative system is approximately obtained. In real life structures, of course, there is always some source of damping present such that the excitation has to be chosen such that it compensates for the damping without having any influence on the motion of the underlying undamped system. For linear structures phase resonance testing is mostly used for an extraction of close or coupled modes or in cases where the modal parameters have to be estimated with the highest possible confidence [19,20]. In linear phase resonance tests the appropriate force vector can often be calculated beforehand with high accuracy based on FRF matrices such that it can directly be applied to the structure and the tuning effort during test is minimized. In the nonlinear case frequency-energy dependence and the lack of the superposition principle makes this generally impossible, such that the appropriate excitation has to be found during the test through successive tuning. Theoretically, the perfect excitation vector for nonlinear phase resonance tests can be derived as follows.

The equation of motion of a mechanical system with conservative nonlinearity can be written as

$$\mathbf{M}\ddot{\boldsymbol{x}}(t) + \mathbf{D}\dot{\boldsymbol{x}}(t) + \mathbf{K}\boldsymbol{x}(t) + \boldsymbol{f}_{\mathrm{nl}}(\mathbf{x}(\mathbf{t})) = \boldsymbol{f}_{\mathbf{exc}}(\mathbf{t}), \tag{1}$$

where $\mathbf{M} \in \mathbb{R}^{m\times m}$ denotes the mass matrix, $\mathbf{D} \in \mathbb{R}^{m\times m}$ the viscous damping matrix, $\mathbf{K} \in \mathbb{R}^{m\times m}$ the linear stiffness matrix and $\boldsymbol{f}_{\mathrm{nl}}(\boldsymbol{x}(t)) \in \mathbb{R}^{m\times 1}$ represents a vector of nonlinear, restoring forces. The vector of external excitation forces is represented by $\boldsymbol{f}_{\mathrm{exc}}(t) \in \mathbb{R}^{m\times 1}$. If it is now desired to enforce a NNM motion of a system governed by Eq. (1), then the response of this forced and damped system must also satisfy the differential equation of the underlying conservative system

$$\mathbf{M}\ddot{\boldsymbol{x}}(t) + \mathbf{K}\boldsymbol{x}(t) + \boldsymbol{f}_{\mathrm{nl}}(\boldsymbol{x}(t)) = \mathbf{0}. \tag{2}$$

Comparing Eqs. (1) and (2), this can only be achieved if the forcing $\boldsymbol{f}_{\mathrm{exc}}(t)$ in Eq. (1) balances out the damping for all times, i.e.

$$\mathbf{D}\dot{\boldsymbol{x}}(t) = \boldsymbol{f}_{\mathrm{exc}}(t), \quad \forall t. \tag{3}$$

Similarly to the approach of Peeters [10], it is now assumed that the motion of the system is periodic and can therefore be described by a Fourier series

$$\mathbf{x}(\mathbf{t}) = \sum_{n=-\infty}^{\infty} \underline{\boldsymbol{x}}_n e^{in\omega t}, \tag{4}$$

where $\underline{\boldsymbol{x}}_n$ denotes the vector of complex Fourier coefficients of the nth harmonic. The assumption of a periodic response to a periodic excitation must generally not hold for nonlinear systems. However, if we seek to measure the NNM motion, which is periodic per definition, then this does not present any limitation. The previous approach [10] was restricted to monophase motions, which implies that not only all degrees of freedom move with the same phase but also all harmonics have the same phase. This assumption limits the subsequent considerations to symmetric nonlinearity, where all harmonics have the same phase, and also excludes phase differences, which may appear in the case of internal resonances [7]. In contrast, the complex notation used in the following allows for such effects. Using Eq. (4) and its derivative with respect to time the damping forces in Eq. (1) can be written as

$$\boldsymbol{f}^{\mathrm{D}}(t) = \mathbf{D}\sum_{n=-\infty}^{\infty} in\omega\underline{\boldsymbol{x}}_n e^{in\omega t} = \mathbf{D}\sum_{n=-\infty}^{\infty} \underline{\boldsymbol{v}}_n e^{in\omega t}, \tag{5}$$

where $\underline{\boldsymbol{v}}_n = in\omega\underline{\boldsymbol{x}}_n$. This means that all harmonics of the damping forces are rotated by $\pi/2$ in the complex plane compared to the displacement. If the excitation forces in Eq. (3) are also assumed to be periodic, then they can be written in the form of a Fourier series as

$$\boldsymbol{f}_{\text{exc}}(t) = \sum_{n=-\infty}^{\infty} \underline{\boldsymbol{f}}_{n,\text{exc}} e^{in\omega t}. \tag{6}$$

Inserting Eqs. (5) and (6) in Eq. (3) yields the condition for the appropriate NNM excitation for every harmonic component individually

$$\underline{\boldsymbol{f}}_{n,\text{exc}} = \mathbf{D}\underline{\boldsymbol{v}}_n, \quad \forall n. \tag{7}$$

Taking into account the phase difference between the damping forces and the displacement as stated in Eq. (5) the phase difference between the excitation and the displacement has to be $\pi/2$ for every DOF and every harmonic individually in order to achieve perfect NNM isolation. This condition is in analogy to linear EMA often referred to as phase lag quadrature criterion. Note that a perfect excitation force appropriation according to Eq. (7) does not only require quadrature for all harmonics but also for all DOFs, which means that a distributed force vector would be necessary depending on the spatial distribution of the damping and the desired NNM shape.

Graphically, the dynamic equilibrium for each harmonic n can be represented as a family of pointers rotating with the angular velocity $n\omega$ in the complex plane as is shown in Fig. 1. For simplicity the pointer diagram is drawn for a cophasal motion in the representative harmonic, i.e. the pointers for all DOFs pointers overlay each other in the complex plane. The application of pointers as a graphical representation of a signal is more common in electrical engineering but was also used e.g. in [21] in the context of multi-frequency excitation of linear mechanical systems. Using this representation it can be seen that in order to achieve a NNM motion, which is depicted in Fig. 1a, the pointer of the excitation force must be shifted by $\pi/2$ in phase with respect to the displacement and be equal in magnitude to the damping forces for each harmonic.

2.1. Modal purity index

The phase lag quadrature relation provides the basis for the nonlinear modal purity index (MPI) proposed by Peeters [22] to assess the quality of the NNM isolation. The MPI is briefly introduced here, as it is used for comparison throughout the paper. Under the assumption of monophase motion, all harmonics of the excitation can be shifted in phase such that they are represented by a purely sinusoidal signal with the respective frequency. Subsequently the response is sought to have a phase lag of $\pi/2$ with respect to the excitation which means that it should be purely cosine shaped. Using a complex notation the modal purity index can be defined for each harmonic individually as

$$\Delta_n = \frac{\Re\{\bar{\underline{\boldsymbol{x}}}_n^{\mathrm{T}}\}\Re\{\underline{\boldsymbol{x}}_n\}}{\bar{\underline{\boldsymbol{x}}}_n^{\mathrm{T}}\underline{\boldsymbol{x}}_n}, \tag{8}$$

where $\bar{\underline{\boldsymbol{x}}}_n$ denotes the complex conjugate of the complex Fourier coefficient $\underline{\boldsymbol{x}}_n$. Accordingly, $\bar{\underline{\boldsymbol{x}}}_n^{\mathrm{T}}$ denotes the Hermitian $\underline{\boldsymbol{x}}_n^{\mathrm{H}}$. The vector $\underline{\boldsymbol{x}}_n$ contains the nth harmonic component of all DOFs of the structure. Eq. (8) represents a response based indicator for the modal purity. In analogy to linear mode indicator functions a value of unity indicates perfect appropriation of the respective harmonic. As a global indicator for the appropriation quality the arithmetic mean of all N harmonic indicators taken into account is used, yielding the global indicator function

$$\Delta = \frac{1}{N}\sum_{n=1}^{N}\Delta_n. \tag{9}$$

In this indicator function the number of harmonics taken into account has to be chosen a priori, e.g. based on observations during experimentation. The value of the MPI can be highly dependent on the number of harmonics considered in the calculation as the phase of higher harmonics with low amplitudes is treated in the same way as harmonics with high amplitudes, even though they might not have significant influence on the NNM motion [18]. In practice, often only the first harmonic is taken into account for the assessment of the modal purity as this is usually the harmonic where the forcing is applied [23]. This might also be misleading, because even for single harmonic forcing the higher harmonics can have significant effects on the NNM motion, e.g. in the case of internal resonances. In the following a more robust and general nonlinear mode indicator function is derived.

3. Power quantities for nonlinear modal testing

For an excitation based assessment of the quality of the NNM isolation the central quantity is the mechanical power of the excitation. The power quantities used in this context are largely based on analogies to power definitions in electrical engineering. Specifically Budeanu's definition of electrical powers in nonlinear systems [24] can be regarded as the foundation of the following derivations. The method can also be regarded as an extension of the so-called reactive power method which can be used in phase resonance testing of linear systems for the measurement of modal parameters and the derivation of the phase lag quadrature criterion [20]. A reactive power related method was also used in [23] for the calculation of the forcing which is necessary for the excitation of a NNM motion in a damped system. In this context it is referred to as Energy Balance Method as all calculations are carried out on an energy level. However, in order to use the Energy Balance Method the sys-

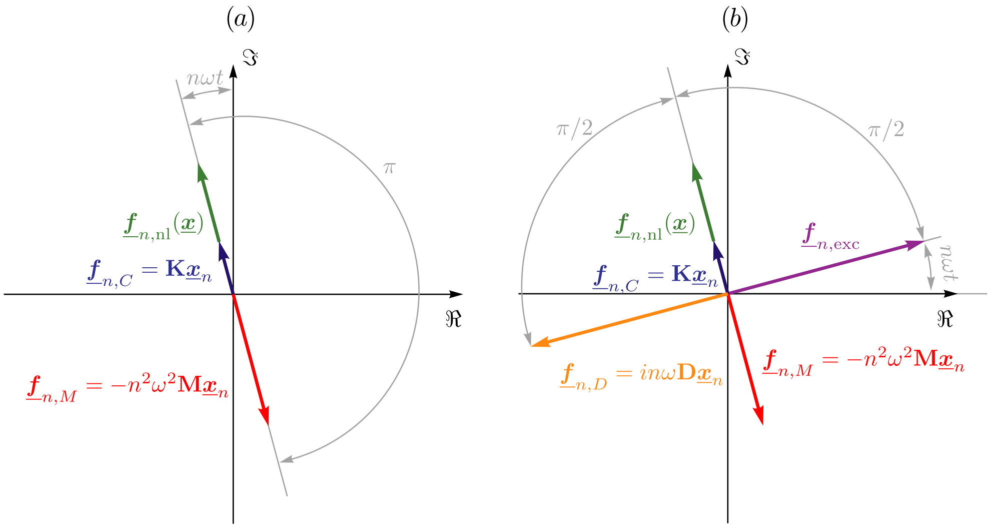

Fig. 1. (a): Pointer diagram for the dynamic force equilibrium for a NNM motion of the conservative system response of a representative harmonic n. (b): Pointer diagram for the dynamic force equilibrium for a NNM motion of the forced response of a representative harmonic n.

tem's matrices, specifically the damping matrix, has to be known a priori. This is obviously not the case if one aims on experimentally identifying the characteristics of an unknown structure as it is done in the present study.

For nonlinear systems the power of the excitation can be related to the NNMs of the underlying conservative system and can therefore also be used as a criterion for the quality of the NNM isolation. The instantaneous mechanical power is defined as the inner product of a force with the velocity. Thus, for the excitation forces the instantaneous power reads as

$$p(t) = \boldsymbol{f}_{\mathrm{exc}}^{\mathrm{T}}(t)\dot{\boldsymbol{x}}(t). \tag{10}$$

The excitation force $\boldsymbol{f}_{\mathrm{exc}}(t)$ is a force in the generalized coordinate space $\mathbb{R}^m$ and therefore a generalized force. The excitation is applied on p physical points on the structure with scalar local forces $\lambda_j(t)$ in generalized force directions $\boldsymbol{w}_j \in \mathbb{R}^m$ for $j = 1 \ldots p$, i.e.

$$\boldsymbol{f}_{\mathrm{exc}}(t) = \sum_{j=1}^{p} \boldsymbol{w}_{\boldsymbol{j}}\lambda_{\boldsymbol{j}}(\boldsymbol{t}), \tag{11}$$

which shows how the individual excitation forces $\lambda_j(t)$ contribute to the generalized force $\boldsymbol{f}_{\mathrm{exc}}(t)$. Then the excitation power in Eq. (10) can be written as

$$p(t) = \sum_{j=1}^{p} \lambda_j(t)\boldsymbol{w}_j^{\mathrm{T}}\dot{\boldsymbol{x}}(t) = \sum_{j=1}^{p} \lambda_j(t)\xi_j(t) = \sum_{j=1}^{p} p_j(t), \tag{12}$$

where $p_j(t)$ represents the instantaneous power of the excitation at the jth excitation point. For the nonlinear modal test it is reasonable to assume that both the excitation forces and the velocity at the excitation points are periodic with some fundamental frequency ω. Hence, these quantities can be represented by complex Fourier series yielding

$$p_j(t) = \sum_{n=-\infty}^{\infty} \underline{\lambda}_{j,n} e^{in\omega t} \sum_{k=-\infty}^{\infty} \underline{\xi}_{j,k} e^{ik\omega t}, \tag{13}$$

where n indexes the harmonic of the forces and k indexes the harmonic of the response. This product of Fourier series can be split into a time-constant part for $n = -k$ and an oscillating part for $n \neq -k$. In analogy to the definitions in electrical engineering the constant part is referred to as active power and can be calculated as

$$P_j = \sum_{n=-\infty}^{\infty} \underline{\lambda}_{j,n}\bar{\underline{\xi}}_{j,n} = \sum_{n=-\infty}^{\infty} |\underline{\lambda}_{j,n}||\bar{\underline{\xi}}_{j,n}| e^{i(\gamma_{j,n} - \vartheta_{j,n})}, \tag{14}$$

where $\gamma_{j,n}$ and $\vartheta_{j,n}$ denote the phase angle of the nth harmonic of the force and velocity and the $|.|$ operator the magnitude of the respective complex coefficient. Using the relation between the complex conjugate coefficients

$$|\underline{\lambda}_{j,n}| = |\bar{\underline{\lambda}}_{j,n}| \quad \text{and} \quad |\underline{\xi}_{j,n}| = |\bar{\underline{\xi}}_{j,n}|, \tag{15}$$

and the fact that the velocity oscillates around a mean value of zero (see Eq. (5)), i.e. $|\underline{\xi}_{j,0}| = 0$ the sum can be rearranged yielding

$$P_j = \sum_{n=1}^{\infty} |\underline{\lambda}_{j,n}||\underline{\xi}_{j,n}|(e^{i(\gamma_{j,n}-\vartheta_{j,n})} + e^{i(-\gamma_{j,n}+\vartheta_{j,n})}) = \sum_{n=1}^{\infty} |\underline{\lambda}_{j,n}||\underline{\xi}_{j,n}|(e^{-i\varphi_{j,n}} + e^{i\varphi_{j,n}}), \tag{16}$$

where $\varphi_{j,n} = \gamma_{j,n} - \vartheta_{j,n}$. This sum can be written in a trigonometric form using Euler's formula yielding

$$P_j = \sum_{n=1}^{\infty} 2|\underline{\lambda}_{j,n}||\underline{\xi}_{j,n}|\cos(\varphi_{j,n}). \tag{17}$$

For convenience, this sum is simplified by the introduction of root mean square values of the nth harmonic component of the force $F_{j,n} = \sqrt{2}|\underline{\lambda}_{j,n}|$ and the velocity $V_{j,n} = \sqrt{2}|\underline{\xi}_{j,n}|$at the jth excitation point to

$$P_j = \sum_{n=1}^{\infty} F_{j,n} V_{j,n} \cos(\varphi_{j,n}). \tag{18}$$

The active power can be interpreted as the mean value of the power brought into the system by the excitation forces over one period, which will be explained in more detail in Section 3.1. Following Budeanu's [24] definition, the reactive power can be introduced as

$$Q_j = \sum_{n=1}^{\infty} F_{j,n} V_{j,n} \sin(\varphi_{j,n}). \tag{19}$$

Note that this definition of reactive power is a based on a rigorous extension of linear theory in the case of harmonic excitation as we will show in Section 3.4 and is not related to a measurable physical quantity. The apparent power can be defined as the product of the total root mean square values of the force F_{RMS} and the velocity V_{RMS}, which can be calculated based on the root mean square values of the individual harmonic components as

$$S_j = F_{\mathrm{RMS}} V_{\mathrm{RMS}} = \sqrt{\sum_{n=1}^{\infty} F_{j,n}^2} \sqrt{\sum_{k=1}^{\infty} V_{j,k}^2}. \tag{20}$$

This definition represents a straightforward extension of linear theory but is also valid without any limitations in nonlinear situations. It is important to notice that the apparent power includes all components of Eq. (13) in an exact way, whereas the active and reactive power only contain parts of the sums with $n = -k$. Therefore, unlike for linear systems with single harmonic excitation, the apparent power cannot be calculated solely based on the active and reactive power. In other words, the power triangular equation well known from linear electrical systems theory turns into an inequality

$$S_j^2 \geqslant P_j^2 + Q_j^2. \tag{21}$$

This inequality can be transformed into the power triangle for the higher harmonic case by the introduction of the distortion power D_j which contains all parts of the sums in Eq. (13) which are not covered by Eq. (14) or Eq. (19) yielding

$$S_j = \sqrt{P_j^2 + Q_j^2 + D_j^2}. \tag{22}$$

This power triangle relation is visualized in Fig. 2 for an example case with three harmonic components. Assume that the system is excited at the fundamental and second harmonic with some arbitrary force. Then the power triangle for the first and second harmonic can be drawn, as it is done in Fig. 2, taking into account the active powers $P_{j,1}$ and $P_{j,2}$ as well as the reactive powers $Q_{j,1}$ and $Q_{j,2}$. Furthermore, there may be a power transfer from one harmonic to another, visualized by the[1] green, dotted vectors $D_{j,1}$ and $D_{j,2}$. Note that there is also the possibility of a power transfer to a harmonic at which no excitation is applied, in this case the third harmonic. Clearly, in contrast to linear systems with single harmonic excitation, the total apparent power S_j is not equal to the Pythagorean sum of the active and reactive power. Additionally, also the power transfer to harmonics which are not excited is included in the apparent power S_j. It becomes obvious that for nonlinear systems the apparent power is a central quantity for the analysis of the excitation forces. The quality of the NNM isolation can be evaluated by relating the active power to the apparent power yielding a power based indicator

$$\Lambda_j := -\frac{P_j}{S_j} \in [-1, 1], \tag{23}$$

which will be explained in more detail in the subsequent sections. Therefore, first of all, it is necessary to relate the derived power quantities for the excitation to the dynamic forces which are relevant in phase resonance testing to explain the relevance of the excitation power considerations.

[1] For interpretation of color in 'Figs. 2 and 12', the reader is referred to the web version of this article.

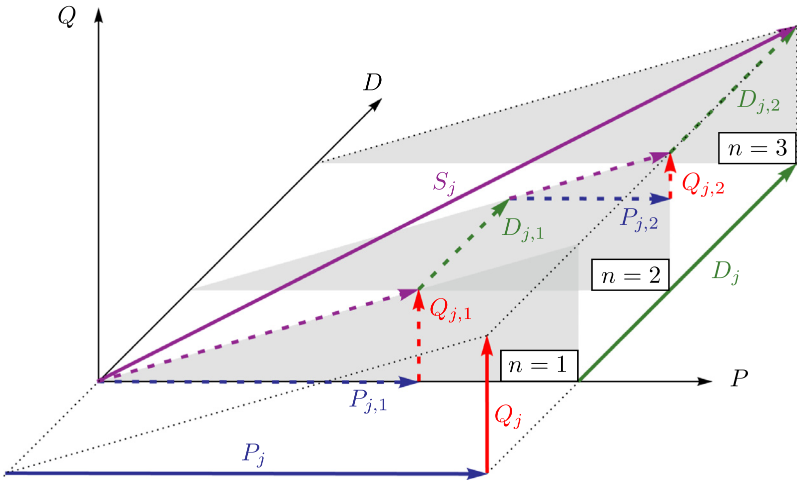

Fig. 2. Power triangle relation for nonlinear mechanical example system.

3.1. Mechanical interpretation of power quantities

The pointer representation introduced in Fig. 1 can be used to associate the previously derived mathematical power quantities to the dynamic force equilibrium introduced in Section 2. For the linear case some of these considerations, particularly for the active and reactive power of single harmonic excitation forces, can be found in [20]. In the nonlinear case a generalization is necessary.

For a representative DOF i all dynamic forces are depicted in individual pointer diagrams along with a pointer of the velocity of the DOF $v_{i,n}$ for a representative harmonic n. Additionally, the complex conjugate pointers for the representative harmonic are introduced, as these play a role for the derivation of active and reactive power. The phase angle between the excitation force and the velocity at the representative DOF is denoted by $\varphi_{i,n}$. The excitation forces at the DOF i are represented in diagram (a) by $f^{\text{exc}}_{i,n}$, the inertia forces in diagram (b) by $f^{\text{M}}_{i,n}$, the conservative restoring forces including linear and nonlinear contributions of the respective harmonic in diagram (c) by $f^{\text{C}}_{i,n}$ and the damping forces in diagram (d) by $f^{\text{D}}_{i,n}$.

The power of each of the forces is the product of the pointers of the velocity and the respective force which can be represented as a pair of two complex conjugate pointers. Hence, a multiplication of these pointers (see Eq. (13)) results in overall two pairs of complex conjugate power components for each harmonic, two of which have a constant phase angle and two rotate with twice the angular velocity of the original pointers. All pointers must compensate one another for all DOFs and all harmonics in the case of a dynamic equilibrium i.e. a steady-state motion. Recall that for the NNM motion the length of the pointers of the excitation force and the damping force is zero, such that the pointers of the power of the inertia forces and the conservative forces balance out. Hence, to ensure a NNM motion of the non-autonomous system the power of the excitation force must balance out the power of the damping forces. This holds for the rotating pointers as well as the pointers with constant phase angle. The real part of the pointers with constant phase is associated with the active power as defined in Eq. (18) and the imaginary part to the reactive power as defined in Eq. (19). Thus, the conservative and inertia forces just contribute to the reactive power, whereas the damping forces just contribute to the active power component of this harmonic. Note that this is the case independent of the phase angle $\varphi_{i,n}$. The only power pointer which can have a contribution to the active and reactive power, dependent on the angle $\varphi_{i,n}$ is the pointer of the excitation power. If the excitation power has a component contributing to the reactive power, then it would clearly affect the dynamic equilibrium between the conservative restoring forces and the inertia forces i.e. the NNM motion. Hence, the phase angle between the excitation force and the velocity must be adjusted in a way that the reactive power of the excitation force disappears. Additionally, it must be enforced that the length of the pointer of the excitation power must be the same as the length of the pointer of the power of the damping forces but with an opposite sign to ensure the dynamic equilibrium for this excitation point. Note that if this is the case, i.e. the angle $\varphi_{i,n} = \pi$, then also the oscillating components of the pointer diagram compensate one another.

For a perfect appropriation of the NNM, the dynamic equilibrium condition must hold for all harmonics and for all m generalized coordinates. This means that for damping forces which are spatially distributed over the whole structure a spatially distributed excitation force would be necessary for perfect NNM isolation. Furthermore, in contrast to linear systems, all harmonics have to be considered. In experiments, it is impossible to realize such an excitation with reasonable effort. However, the derived power quantities can still be used to assess the quality of the NNM isolation, especially in the case of an imperfect appropriation. For points and harmonics at which an excitation is applied, the phase of the excitation can be evaluated by inspection of the reactive power. If additionally the pointers of the excitation forces and damping forces are equal in magnitude, then no power is transferred to different points or different harmonics and the distortion power also disappears. For points where no excitation is applied, the active power of the excitation is zero, such that the dissipated power at these points must theoretically also be zero in the case of an NNM motion. If this is not the case, additional power has to be introduced at the excitation points to ensure power balance for the total structure. In this case the dynamic equilibrium at the excitation points would be affected and the distortion or reactive power would not be zero. This means that by regarding the excitation points, the quality of the NNM appropriation can be evaluated for the whole structure.

3.2. Power based mode indicator function

As already stated for an ideal compensation of the damping without any influence on the NNM motion the mean value of the power of the excitation has to be located on the real axis for all harmonics (see Fig. 3a and d). In this case the reactive power of the excitation vanishes such that

$$Q_j = \sum_{n=1}^{\infty} F_{j,n} V_{j,n} \sin(\varphi_{j,n}) = 0. \tag{24}$$

If additionally the magnitudes of the pointers for the excitation and the damping powers are equal for all harmonics and DOFs individually there is no power transferred from one harmonic to another or to different points on the structure, then the total power brought into the system over one period is equal to the active power observed at the excitation point:

$$S_j = |P_j|. \tag{25}$$

This also means that according to the nonlinear power triangle relation (see Eq. (22)) the distortion power disappears:

$$D_j = 0. \tag{26}$$

Note that the active power (see Eq. (18)) has a sign depending on the angles $\varphi_{j,n}$, whereas the apparent power is positive per definition (see Eq. (22)). The sign of the active power is negative in the vicinity of a mode:

$$\varphi_{j,n} \approx \pi \quad \forall n \quad \Rightarrow \quad \cos(\varphi_{j,n}) < 0. \tag{27}$$

By relating the apparent power to the active power, the quality of the excitation can be assessed. Hence, the power based mode indicator function (PBMIF) Λ_j for the jth excitation point is defined as

$$\Lambda_j := -\frac{P_j}{S_j} \in [-1, 1], \tag{28}$$

The negative sign is chosen for the sake of consistence to linear MIFs and the MPI which usually gives results of 1 in the case of perfect NNM isolation. If the PBMIF is close to unity, then the excitation is appropriate for the extraction of an NNM. This provides an easy to use indicator, as only the velocity and the force at the excitation point have to be measured, which can be implemented little experimental effort. The calculation of the corresponding power quantities and the PBMIF is straightforward.

3.3. Interpretation of the PBMIF in the time domain

In the previous sections the power components and the PBMIF are derived in the frequency domain. This is the most common way to derive power quantities in electrical engineering and it is consistent with the previous works regarding linear and nonlinear phase resonance testing in structural dynamics. However, it should be noted, that the derivation of the PBMIF is also possible in the time domain, where the active power P_j at excitation point j can be calculated as

$$P_j := \frac{1}{T}\int_0^T \lambda_j(t)\xi_j(t)dt. \tag{29}$$

This quantity represents the mean value of the power input to the system over one period. The apparent power S_j is defined in the time domain as

$$S_j := \sqrt{\frac{1}{T}\int_0^T \lambda_j^2(t)dt}\sqrt{\frac{1}{T}\int_0^T \xi_j^2(t)dt}, \tag{30}$$

which can be interpreted as the norm of the function of the excitation force multiplied with the norm of the function of the velocity at the excitation point. Then the PBMIF can be interpreted based on the Cauchy-Schwarz inequality:

$$\sqrt{\int_0^T \lambda_j^2(t)dt \int_0^T \xi_j^2(t)dt} \geqslant \left|\int_0^T \lambda_j(t)\xi_j(t)dt\right| \quad \text{or } S_j \geqslant |P_j|. \tag{31}$$

If the active power P_j is equal in magnitude to the apparent power S_j, then the equality in Eq. (31) holds and the PBMIF defined in Eq. (28) is equal to unity. This is the case if the excitation forces and the damping forces have the same functional form and are related by a time constant scaling factor. If the functions are expanded by means of a Fourier series, then the

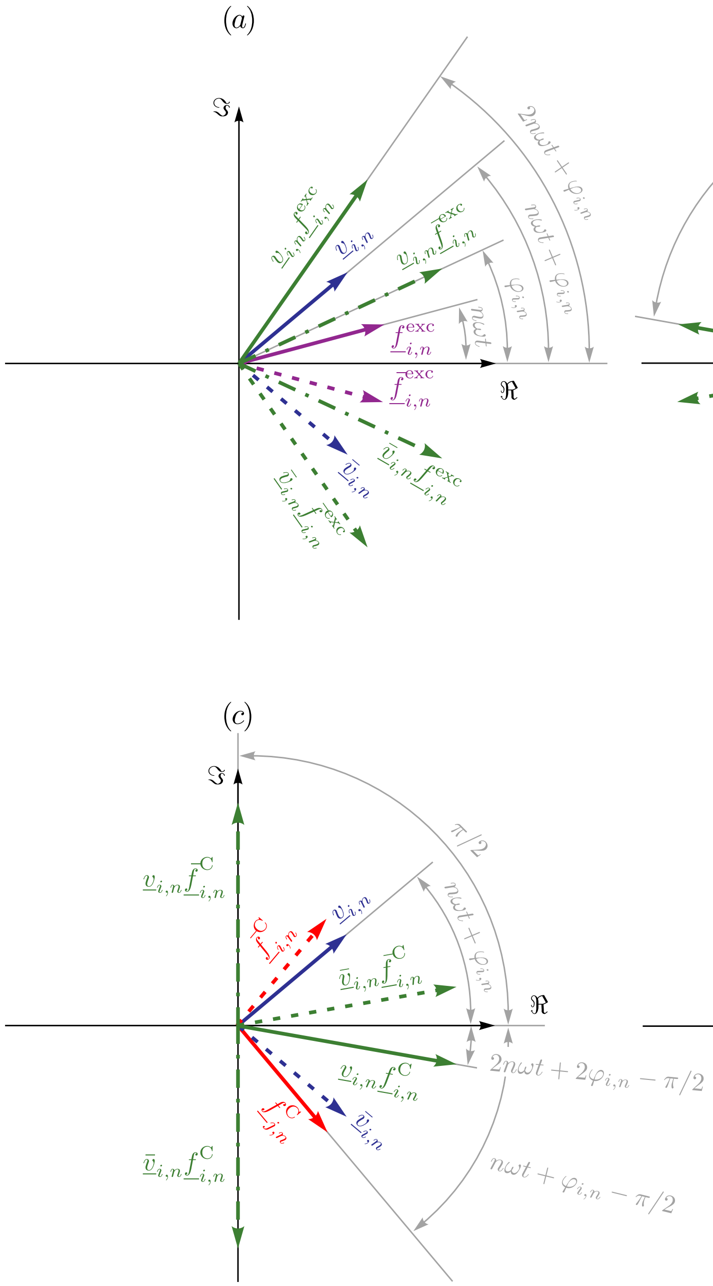

Fig. 3. (a): Pointer diagram of excitation forces. (b): Pointer diagram of inertia forces. (c): Pointer diagram of conservative restoring forces. (d): Pointer diagram of damping forces.

frequency domain formulation follows from Parseval's theorem. Up to this point both derivations are fully equivalent. However, the treatment of the excitation power properties in the frequency domain additionally provides a definition for the reactive and distortion power, which cannot be obtained in a straightforward way by the derivation in the time domain.

3.4. Relation to linear systems

For linear modal analysis the mechanical power was used previously for the derivation of the phase lag quadrature criterion [20]. In this context, the reactive power is used as a measure for the mode appropriation. Furthermore, modal properties like the modal mass and damping can be estimated directly based on the stationary reactive power criterion. This methodology cannot be directly transferred to nonlinear systems, essentially because the reactive power is a purely mathematical quantity with limited physical meaning in nonlinear systems. For illustration, consider the single harmonic case where the mechanical power Eq. (13) can be transferred into the form

$$p_j(t) = F_{j,1}V_{j,1}\cos(\varphi_{j,1}) + F_{j,1}V_{j,1}\cos(\varphi_{j,1})\cos(2\omega t) + F_{j,1}V_{j,1}\sin(\varphi_{j,1})\sin(2\omega t). \tag{32}$$

Using the definitions of the active and reactive powers (see Eqs. (14) and (19)) the instantaneous power is fully represented by these to two quantities:

$$p_j(t) = P_j + P_j\cos(2\omega t) + Q_j\sin(2\omega t). \tag{33}$$

Owing to this it is sufficient to consider the reactive power to investigate the effectiveness of the excitation. Additionally, the apparent power S_j can be calculated as the Pythagorean sum of the reactive and active power yielding

$$S_j = F_{j,1}V_{j,1} = \sqrt{P_j^2 + Q_j^2}. \tag{34}$$

Hence, the apparent power is fully described by the active and the reactive power and a disappearing reactive power implies equality of apparent and active power. However, this relationship does not hold in the multi-harmonic case, as it was stated in Eq. (22) and visualized in Fig. 2. In this case the reactive power has limited meaning, because it does not resemble the effect of power transfer between different harmonics. Theoretically, the reactive power can vanish completely but the mode is still not isolated correctly. In Fig. 2 the pointer of the apparent power S would then lie in the P-D plane but generally not on the P-axis. This would be the case, if the phase lag between excitation and response for all harmonics was $\pi/2$ at the excitation point but the apparent power was not equal to the active power due to power transfers. Hence, it is crucial to regard the relation of apparent and active power in nonlinear systems instead of the reactive power.

3.5. Remarks on Budeanu's power definition

It should be noted that the limited physical meaning of the reactive power for nonlinear systems is also the reason why there is still a vivid discussion in electrical engineering about the definition of the reactive power and their applicability. There are different definitions of reactive power, whereas the definition of active and apparent power are more or less consensus [25]. Indeed, Budeanu's definition is controversial for applications in electrical engineering like power measurements [26]. Still, the choice of Budeanu's definition as a basis for the application in nonlinear modal testing is reasonable mainly due to two reasons. Firstly, it is a direct extension of the linear systems theory which is familiar to most practitioners. Moreover, the linear theory was applied to linear mechanical systems before and the new method for nonlinear modal analysis is fully consistent with this approach. Secondly, although the concepts of reactive and distortion power are purely mathematical constructs in Budeanu's framework, they can be calculated based on experimental data and related to physical effects in the context of nonlinear modal analysis. High reactive power indicates a poor compliance of the phase criterion which can even be localized to a certain harmonic. High distortion power shows a strong influence of power transfers to higher harmonics and other DOFs, which can be reduced by improving the appropriation quality of higher harmonics or the spatial distribution of the forcing. In conclusion, Budeanu's definition provides a clear theoretical framework as well as practical guidelines for the experimentalist in the context of experimental nonlinear modal testing.

3.6. Global indicator for multi-point excitation

The extension of the PBMIF concept to multi-point excitation, e.g. in the case of multi-shaker excitation, is straightforward. The criteria derived for a single excitation point j must be satisfied for all excitation points individually in order to obtain a NNM motion. Hence, the reactive power for all excitation points must disappear individually:

$$Q_j = \sum_{n=1}^{\infty} F_{j,n}V_{j,n}\sin(\varphi_{j,n}) = 0, \quad \forall j. \tag{35}$$

This means that the phase criterion is fulfilled for all excitation points and all harmonics. Furthermore, the distortion power D_j must also disappear in the case of a perfect NNM appropriation yielding:

$$S_j = |P_j|, \quad \forall j. \tag{36}$$

In this case there is no power transferred from one excitation point to another excitation point, because the dynamic equilibrium holds for all excitation points individually. As a result the PBMIF for all p excitation points must be equal to unity in the case of perfect NNM isolation. Therefore, a global indicator for the NNM appropriation in the case of multi-point excitation can be defined as

$$\Lambda := \frac{1}{p}\sum_{j=1}^{p}\Lambda_j \in [-1, 1], \tag{37}$$

which is unity in the case of perfect NNM appropriation. This choice for a global indicator in the case of muli-point excitation is motivated by the fact that the power balance must hold for all points individually for perfect NNM appropriation, as explained in Section 3.1.

4. Phase-locked-loop for backbone curve tracking

For phase resonance testing the phase of the excitation has to be adjusted with respect to the response. In the first approaches of nonlinear phase resonance testing [10] the phase is adjusted manually by changing the excitation frequency of the fundamental harmonic of the excitation, which is a challenging procedure. Recently, Renson proposed to use control based continuation methods [27] to make the tuning process more robust. In both cases, only the phase of the fundamental harmonic component is considered. This implies the influence of the phase and amplitude of the higher harmonics is assumed to be negligible for the NNM isolation. This assumption was found to provide reasonably accurate results in experimental tests and is also the basis for the following control algorithm. In this paper, a PLL controller is used for a direct and automated tuning of the phase of the fundamental harmonic force. Compared to the previous methods this controller provides the advantages of being robust and very fast. The PLL controller is a concept well known in radio technology and electrical engineering. The PLL is a nonlinear oscillator, which generates a harmonic signal with a frequency which is tuned based on the phase difference with respect to a reference signal. Generally, the PLL consists of three blocks, namely the phase detector, the loop filter and the voltage controlled oscillator (VCO). The structure of the PLL is shown in Fig. 4. There are many different implementations of the PLL for different applications and a detailed review of these is beyond the scope of this paper. The interested reader is referred to the numerous references about the design of PLLs [28–30]. The implementation used for nonlinear modal testing is briefly sketched in the following and the tuning of the controller for this purpose is addressed on the basis of a numerical example in the next section.

The first block of the PLL is the phase detector which extracts the phase of the output of the system with respect to the reference signal. In the following a mixing phase detector is used which is comparing a reference signal $r(t)$ with the output of the PLL $u(t)$ by a multiplication yielding

$$w(t) = r(t)u(t). \tag{38}$$

For the nonlinear modal analysis the displacement $x(t)$, velocity $\dot{x}(t)$ or acceleration $\ddot{x}(t)$ can be used as a reference signal depending on which quantity is measured. However, as was shown by Fan [31] it is advantageous to modify the signal of, for instance the displacement, by replacing it with its sign

$$r(t) = \operatorname{sign}(x(t)) = \begin{cases} -1 & x(t) < 0 \\ 1 & x(t) \geqslant 0. \end{cases} \tag{39}$$

This modification can be regarded as a sort of amplitude normalization of the reference signal. On the one hand this is advantageous when the reference signal is small in amplitude, e.g. in regions which are far from resonance. Then the normalization leads to an amplification which increases the speed of the PLL. On the other hand the stability criteria for the controller become independent of the amplitude [31]. Both properties are advantageous in the context of nonlinear modal testing, as the system is a priori unknown, such that the location of resonances and amplitude values at specific frequencies cannot be estimated beforehand. The multiplication of the reference with the PLL output signal yields an output of the phase detector which consists of a constant component, which is a function of the phase difference of the input signals θ_e, and an oscillating component. The output of the phase detector is passed to the second part of the PLL, the loop filter, consisting of a low pass filter and a proportional-integral (PI) controller. The low pass filter is described by the differential equation

$$\frac{1}{\omega_l}\dot{e} + e = w(t), \tag{40}$$

with the cutoff frequency ω_l. The idea of the low pass filter is to suppress all oscillating terms of the output of the phase detector in Eq. (38). Thus, the output of the low pass filter $e(t)$ is solely a function of the phase error θ_e. The signal $e(t)$ is then used as a control input of a PI-controller that can be described by the state space model

$$\begin{aligned} \dot{z} &= e \\ y &= K_P\left(e + \frac{1}{T_i}z\right). \end{aligned} \tag{41}$$

The parameters K_P and T_i are the tuning parameters of the proportional and integral part of the controller. The PI-controller provides the control signal for the third part of the PLL, the Voltage-Controlled-Oscillator (VCO), that generates a harmonic signal for the excitation of the structure. The VCO uses the fact that the frequency is the derivative of the phase. Hence, the instantaneous phase can be obtained by an integrator

$$\theta_v = \int_0^t \omega_c + y(\tau) d\tau, \tag{42}$$

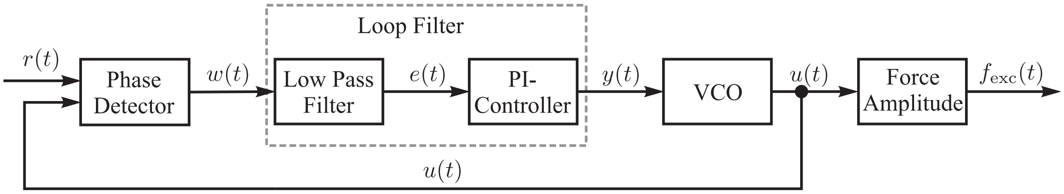

Fig. 4. Schematic structure of PLL controller.

with the center frequency ω_c. The center frequency ω_c is the frequency with which the VCO oscillates in an open loop state. The output of the VCO is generated by inserting the instantaneous phase into a cosine function:

$$u(t) = \cos(\theta_v). \tag{43}$$

The cosine function is used to shift the phase by $\pi/2$ compared to the reference signal, i.e. the displacement. A sine function would yield a synchronous oscillation of the output with the reference signal. The signal $u(t)$ is firstly fed back into the phase detector and secondly multiplied by the excitation amplitude $\hat{f}_{\text{exc}}$ yielding the excitation force

$$f_{\text{exc}}(t) = \hat{f}_{\text{exc}} u(t), \tag{44}$$

which is applied to the structure. Once the phase difference is successively minimized by the controller, the PLL is said to be in a "locked state". The practical application of the PLL for nonlinear modal testing and the tuning of the PLL parameters is addressed by a numerical example in the next section.

4.1. Remarks on phase-control

In most structural dynamics applications frequency-controlled measurements are used to experimentally investigate the system of interest, i.e. the frequency of excitation is preset by the external source of excitation and the response is measured. By the use of the PLL the phase of the excitation is controlled and the frequency of excitation is the result of the response of the system, which is used as feedback in the control circuit. The vibratory system together with the controller can thus be regarded as an autoresonant system. This type of excitation provides several advantages for testing near resonance, which are investigated by Sokolov [32] through detailed analytical studies of academic examples. The most relevant findings of these analytical studies for nonlinear modal analysis can be explained based on the amplitude-phase relation of the system. In contrast to the FRF (see Fig. 6a), which is classically considered in structural dynamics, the phase-amplitude relation (see Fig. 6b) is single-valued, at least locally around a resonance. This means that if it is possible to control the phase lag of the response with respect to the excitation to a certain value, then a unique point of the response curve is obtained. Moreover, the phase amplitude relation is also bell-shaped with a flat region in the vicinity of the resonance, whereas especially for lightly damped systems the FRF has a sharp peak at resonance. As a consequence perturbations of the phase only have small influence on the response amplitude, whereas perturbations of the frequency have strong influence and can even lead to jumps in amplitude. The single-valuedness and flatness of the phase amplitude relation has the following advantages:

- All points of the FRF can be measured if the phase is controlled successfully. Even unstable periodic solutions can be stabilized and measured in experiments using phase-control [33].
- For weak damping, phase-control simplifies maintaining the resonant vibration. Small phase errors have minor influence on the measured amplitude response.

Sokolov also shows that the flatness and single-valuedness of the phase-amplitude relation is largely independent of most relevant system parameters like the damping coefficients, forcing amplitudes and even nonlinear restoring forces. This makes phase-controlled or autoresonant systems particularly interesting for maintaining resonant vibrations of weakly damped systems, which is, for instance, exploited in frequency modulated atomic force microscopy [34] or ultrasonically assisted machining processes [35]. For the application of nonlinear EMA, where unknown, weakly damped, nonlinear systems are the subject of interest, these properties are particularly beneficial.

5. Numerical example for PLL method

This section considers a numerical example to illustrate the methodology of phase resonance testing with the PLL method and assess the quality of the results. The objective of this numerical study is twofold: first, the tuning of the PLL controller is investigated, such that the robustness of the method can be illustrated. Second, the actual NNM cannot be obtained in an experiment such that it is difficult to evaluate the quality of the results on this basis. For this reason the results of the PLL method are compared to the results of numerical continuation of the NNM. The numerical test structure consists of the FE-model of a beam which is fixed on one end and supported by a nonlinear spring, with linear and cubic spring stiffness, on the other end. A schematic sketch of the structure is shown in Fig. 5. The FE-model consists of seven Euler–Bernoulli beam elements and features in total 21 DOFs. For the forced response and the PLL test the structure is excited at the second node by a harmonic function. At the tip of the beam, similarly to the following experimental study, a constant preload can be applied. The linearized system matrices **M** and **K** including the static preload are calculated by a nonlinear static FE-calculation. The preload is chosen such that the structure can be tested in the highly nonlinear range without the influence of internal resonances. The damping matrix is assumed to be proportional of the form

$$\mathbf{D} = \alpha_1 \mathbf{M} + \alpha_2 \mathbf{K}, \tag{45}$$

where $\alpha_1 = 1$ and $\alpha_2 = 10^{-5}$ are chosen such that the damping is weak and resembles the ones observed in similar experiments. The parameters of the numerical model are listed in Table 1.

The procedure of phase resonance testing with the PLL method is illustrated in Fig. 6a. The test is started at a low excitation level at a specific center frequency of the VCO $f_c = \omega_c/2\pi$. The PLL automatically adjusts the forcing frequency based on the phase difference to the first harmonic of the response, which is referred to as "PLL tuning". Once the phase difference is $\pi/2$, i.e. a mode is reached, the PLL is in the locked state, generating a harmonic signal with a specific frequency f. The response of the system is then assumed to be approximately on the backbone curve and the data is recorded. Once this is done, the force level is incrementally increased. The higher forcing level leads to a higher energy input into the system and in the case of a nonlinear structure the NNM frequency may depend on the energy. Thus, the excitation frequency has to be adapted to be able to appropriately excite the NNM, i.e. to meet the phase criterion. This is automatically done by the PLL as the controller is always tuning the frequency such that the phase lag of the the first harmonic is $\pi/2$. As soon as the locked state of the PLL is reached, a new data point on the backbone curve can be recorded. This procedure is repeated until a desired forcing level is reached.

As derived in Section 4, there a several parameters in the PLL controller which need to be tuned. This tuning has to be done in a heuristic way, which makes it important to show that the procedure is generally robust in a wide parameter range. Especially for the use in nonlinear system identification, it is desired to be able to perform measurements with minimal previous knowledge of the structure. First of all, the stability bounds of the controller can be determined, e.g. using Lyapunov methods [28], yielding the following restrictions for the parameters:

$$K_P, \omega_l, \quad \frac{1}{T_i} > 0 \quad \text{and} \quad \omega_l > \frac{1}{T_i}. \tag{46}$$

The cutoff frequency of the low pass filter ω_l is usually chosen to be much lower than the expected NNM frequency, because one aims at suppressing all oscillating components of the output of the phase detector. In all numerical and experimental studies within this paper the frequency is set to $\omega_l = 2\pi$ rad/s, which is approximately 2–3% of the lowest natural frequency of the beam. The tuning parameter of the integral part of the controller has to be positive but smaller than ω_l and its influence on the performance of the PLL was found to be small such that a detailed numerical study of this parameter is omitted. In the numerical and experimental studies this parameter was set to $T_i = 2/\omega_l$. Subsequently some simulation results are shown to illustrate the influence of the remaining tuning parameters K_P and ω_c. Firstly, the proportional factor K_P is investigated by the simulation of a specific test case with varying values for K_P. The test case consists of two measured points on the backbone curve: One point for an excitation level of $\hat{f}_{\mathrm{exc}} = 0.5$ N which yields a response which is approximately in the linear range of the first mode. Then the excitation is stepped up to $\hat{f}_{\mathrm{exc}} = 2$ N which is already in the nonlinear range. The tuning time which is required for the measurement of this test case is shown in Fig. 7 for different tuning factors K_P. It can be observed, that the PLL test is successful for the whole parameter range and tuning time decreases with increasing value of K_P. However, in a parameter range from $K_P > 50$ the tuning time stabilizes around 10 s for this test case. The factor K_P amplifies the output of the loop filter. If its output is biased by noise, then a high value of K_P may increase the sensitivity of the PLL to noise. In the following experimental study it was observed that the measurement noise did not significantly affect the functionality of the PLL. Another factor influencing the reaction time of the PLL is the cutoff frequency of the loop filter ω_l. The cutoff frequency is held constant for the comparability of the performance of the PLL for different values of K_P. However, it should be noted that the total tuning time is influenced by both parameters. The numerical study illustrates that the performance of the PLL is not very sensitive to the tuning of the PI-controller, which is important if one aims on investigating unknown structures. Similar behavior was also observed in different numerical as well as experimental studies and also reported in [33] for a slightly different implementation of the PLL. A second numerical study is carried out to illustrate the influence of the center frequency. Therefore, the structure was tested at a low excitation level of 0.5 N as it is usually done for finding the first point of the backbone curve. The center frequency of the PLL is varied from 5 Hz to 155 Hz. Fig. 7 shows the FRF of the beam in this frequency range and the response for the investigated center frequencies. After the PLL reaches a locked state, the respective point on the FRF is calculated again. It can be observed that the PLL is able to find the first mode for all starting points marked in blue and the second mode for the starting points marked in red. It can be clearly seen that independently of the center frequency a mode is found by the controller. Whether the PLL locks to the first or second resonance, solely depends on the location of the anti-resonance which separates the two modes in the FRF. This shows that generally no a priori knowledge about the eigenfrequencies of a structure is necessary to carry out the nonlinear modal test with the PLL method.

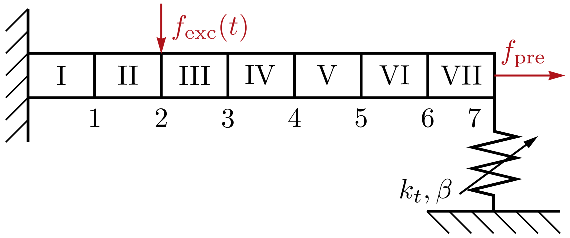

Fig. 5. FE-model of the numerical beam structure.

After these preliminary considerations about the tuning of the PLL controller, the numerical study assesses the capability of the controller to keep track of the backbone curve, the speed and the accuracy of the method. Therefore, the complete backbone curve is tracked for the example system for forcing values from 0.5 N to 8 N. The excitation level is incremented in steps of 0.25 N yielding in total 31 measured points. The total time required for this test, including tuning and measurement times, is 250 s. The results of the PLL test are transformed into the frequency domain with a Fast Fourier Transform (FFT) and compared to the simulated backbone curve and FRF in the three dimensional frequency-phase-amplitude space in Fig. 8. To avoid leakage effects in the FFT, an integer multiple of the period length of the excitation signal can be chosen for the analysis here and in the following evaluations of the PBMIF. The same approach can be used for the experimental evaluation as the excitation frequency is a known output of the PLL. The backbone curve was calculated by solving Eq. (2) and the FRF by solving Eq. (1). Both calculations were carried using the harmonic balance method taking into account nine harmonics and the first harmonic component is displayed. For the details of the numerical method see [36]. It can be seen that the results for the first harmonic of the PLL method perfectly agree with the first-order simulated backbone curve and FRF results. Apparently, the NNM seems to be isolated very well even with a single harmonic, single point force. However, to be able to judge the quality of the NNM isolation, also the level and the phase of the higher harmonics has to be evaluated. Therefore, the new PBMIF Λ is calculated for each measured point as well as the MPI proposed by Peeters [10]. The MPI can be calculated in this case, because a monophase motion of the NNM is expected due to symmetric nonlinearity and the absence of internal resonances. As already discussed in Section 2, the number of harmonics considered in the MPI has to be chosen beforehand. In this test firstly only the fundamental harmonic MPI is considered, denoted by Δ_1. Secondly, the MPI Δ_{10} is calculated, taking into account all harmonics which reach a relative amplitude of 10% of the fundamental harmonic. In contrast, no preliminary assumptions have to be made for the PBMIF made, as all frequencies are naturally taken into account. The results in Fig. 8 show the comparison of these three measures. The value of Δ_1 indicates a perfect NNM isolation, which means that all DOFs vibrate in phase for the first harmonic and with a phase lag of $\pi/2$ compared to the excitation. However, this is still inconclusive for the assessment of the influence of higher harmonics. If one takes into account higher harmonics and calculates Δ_{10}, then there is a large variance from one measured point to another, which is basically due to two reasons. First, the phase of the higher harmonics is not controlled and thus solely depends on the phase response of the system. Second, the Δ_{10} is calculated as a arithmetic mean of MPIs for each individual harmonic. Thus, small amplitudes of higher harmonics are weighted in the same way as the fundamental harmonic. Clearly, neither of these measures is conclusive to assess the quality of the NNM appropriation. In contrast, if one regards the results for the PBMIF, then the picture becomes clear. For low level excitation Λ is close to unity, which is reasonable as higher harmonics do not play a role in the almost linear range and the first harmonic results are very close to the backbone curve. For higher excitation levels the value of Λ decreases to approximately 0.95, which still indicates a very good NNM approximation. The small deviation from unity in this case is caused by the distortion power component of Eq. (22) as for single harmonic forcing neither the active power P nor the reactive power Q have higher harmonic content. Furthermore the reactive power of the fundamental harmonic Q_1 is also close to zero because the phase angle of this harmonic is close to $\pi/2$. This also makes the need for the evaluation of the apparent power S clear if one seeks to evaluate the quality of the NNM isolation.

6. Experimental results

To demonstrate the applicability of the proposed method an experimental study is carried out. The subject of this study is a clamped steel beam with a thin steel beam at its tip, which is also clamped. This beam structure is similar to the so called

Table 1
Parameters of numerical beam structure.

Parameter	Value	Unit
E	185	GPa
ρ	7830	kg/m^3
β	8×10^9	N/m^3
k_t	1000	N/m
f_{pre}	500	N

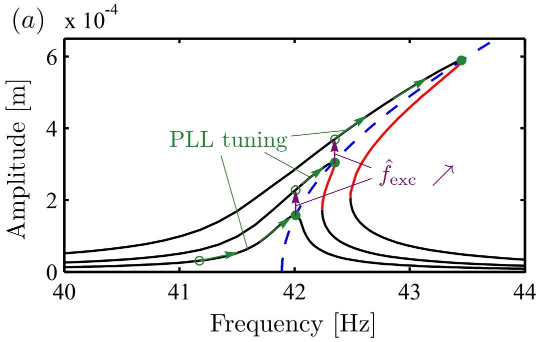

Fig. 6. (a): Demonstration of PLL method in the frequency-amplitude domain. (b): Demonstration of PLL method in the phase-amplitude domain.

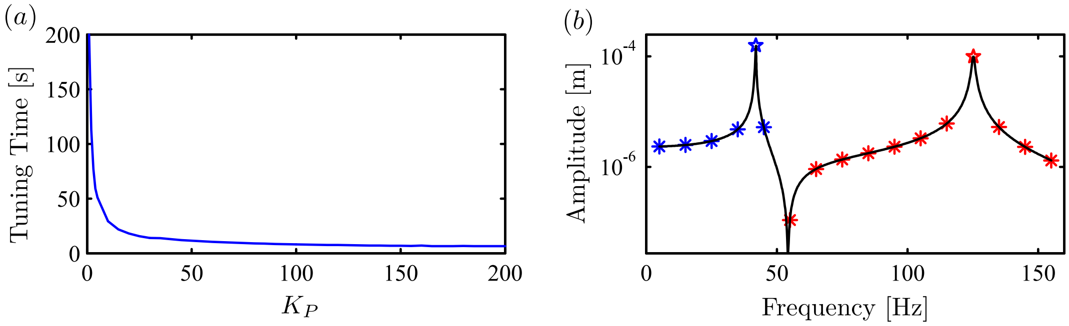

Fig. 7. (a): Tuning time for PLL test case depending on the parameter K_P. (b): FRF of beam structure and different starting points (*) and end points (☆) for varying center frequencies of the VCO (blue, locked to first mode, red locked to second mode). (For interpretation of the references to color in this figure legend, the reader is referred to the web version of this article.)

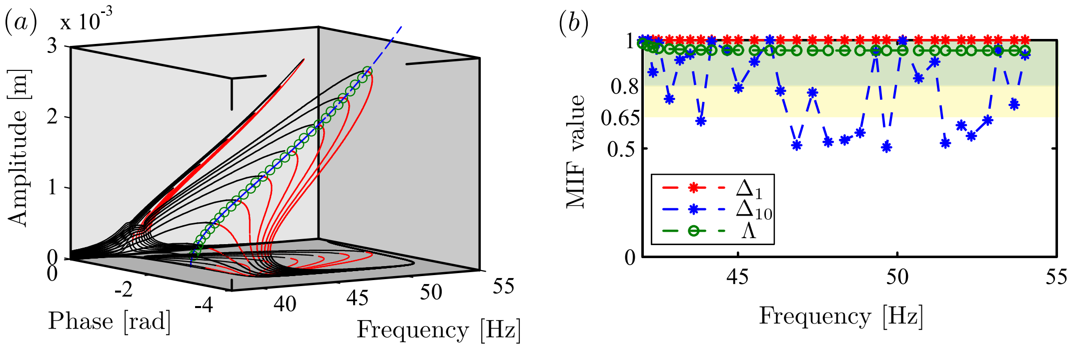

Fig. 8. (a): First harmonic of numerical PLL test (o), simulated backbone curve (- -) and forced response in frequency-phase-amplitude space with projections onto FRF and phase-response plane (black: stable, red: unstable). (b): Fundamental harmonic MPI Δ_1, higher harmonic MPI Δ_{10} and PBMIF Λ. (For interpretation of the references to color in this figure legend, the reader is referred to the web version of this article.)

"ECL beam" which was proposed by Thouverez [37] in 2003 and subsequently used in various configurations as a benchmark for nonlinear system identification by numerous researchers [38,10,39]. A photo of the test rig used in this paper is shown in Fig. 9.

The clamping mechanism of the small beam is moveable to adjust the pretension f_{pre} of the specimen. The pretension can be measured using a full bridge circuit of strain gauges applied to the thick beam. This mechanism is primarily used to avoid buckling phenomena (e.g. due to thermal expansion of the setup). The structure is excited by an electrodynamic shaker and the response is measured using in total seven accelerometers. The force at the excitation point $f_{exc}(t)$ is measured by an impedance head. The PLL controller and all data acquisition functions are implemented on a DSpace 1103 rapid prototyping system. The control is based on the force $f_{exc}(t)$ and the reference acceleration $\ddot{x}_{ref}(t)$ measured at the excitation point and the output of the DSpace system is amplified and used as input voltage $v(t)$ for the shaker. A schematic sketch of the experimental setup is shown in Fig. 10. Note that unlike in the numerical study the force amplitude cannot directly be preset in the

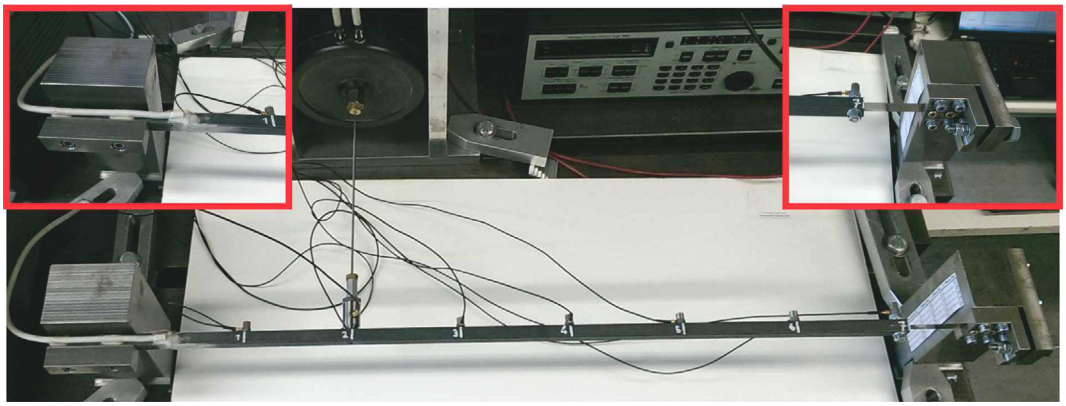

Fig. 9. Photo of the test rig used for the experimental study.

experiment, because the actual force at the excitation point is the reaction force between the shaker and the structure at a specific input voltage. However, the measured force can still be used as control input for the phase control of the output voltage. The amplitude level of the output voltage is incrementally stepped up from low to high during the test until a critical force level is reached. This provides the advantage that no additional effort has to be made to control the force amplitude which simplifies the control algorithm and reduces the measurement time. Nevertheless, the PLL controller can be combined with amplitude control if this is desired. The optimal choice of the reference acceleration for the PLL controller is generally not a priori known. Clearly, the reference node should not be located near a nodal line of the vibration mode of interest, because then obviously the reference signal would be very small and possibly biased by noise. A natural choice is the point of excitation as reference node because at this point all excited modes can also be measured. The linear modes of the beam can be shifted within certain bounds by adjusting the pretension of the setup. The linear eigenfrequencies of the first two modes depending on the pretension of the setup are shown in Fig. 11a. The nonlinearity which is caused by the large displacement of the thin beam at the tip has the largest influence on the first mode. This mode is therefore chosen for the experimental demonstration. The influence of the nonlinearity decreases with increasing pretension as the tip displacement of the thick beam also decreases. Furthermore, the ratio of the first two eigenfrequencies can be changed such that internal resonances can be avoided for the test case. Based on these considerations, the first mode is chosen for the test, with a small tensile pretension in the setup of 20 N to avoid buckling but to have the largest possible influence of the nonlinearity without an internal resonance. For the test the input voltage of the shaker is incrementally increased over time as is shown in Fig. 11b, yielding an increasing excitation force. The total time required for the measurement including tuning times and measurement times is 236 s. Fig. 12a shows the backbone curve which was obtained by the PLL test (green circles). Obviously, the system shows a strong stiffening behavior and the NNM frequency is shifted by almost 20% while the excitation is stepped up. To evaluate the relation between the measured points on the first-order backbone curve and the associated NNM, the same mode indicator functions as in the previous section are evaluated in Fig. 12b. Therefore, all measured points are taken into account for the calculation of the MPI, whereas only the excitation point needs to be evaluated to obtain the PBMIF. Because a single excitation point is used, we omit the index of the excitation point j for brevity. First of all, the value of the fundamental harmonic MPI Δ_1 is close to unity even in the highly nonlinear range. This shows that the phase lag of the fundamental harmonic response of all measured points is approximately $\pi/2$ with respect to the fundamental harmonic of the force. Clearly, the PLL is capable of keeping track of the nonlinear backbone curve of the first harmonic. However, as discussed previously, it does not necessarily mean that the NNM is appropriated perfectly. If one considers higher harmonics with a relative amplitude of 10% or more in the MPI Δ_{10}, then the results become ambiguous as Δ_{10} keeps moving from high to low values for increasing frequency. This once again shows that the MPI is highly dependent on the number of harmonics taken into account, which makes it difficult to evaluate the overall quality of the NNM appropriation. In contrast, the PBMIF automatically takes into account all frequencies and it becomes clear that the for larger amplitudes the value of the PBMIF decreases successively. Compared to the MPI, the PBMIF shows a clear trend that indicates that the fundamental harmonic forcing might not be sufficient to isolate the NNM with high confidence in the frequency range above 28.5 Hz. The analysis of the excitation power components shown in Fig. 13 provides a conclusive explanation for the decrease of the PBMIF for higher amplitudes. In Fig. 13a the fundamental and third harmonic component of the reactive power, denoted by Q_n, related to the active power of the fundamental harmonic P_1 are shown. The other harmonic components of the reactive power were found to be negligible. It can be seen that the reactive power of the fundamental and third harmonic is also comparably small. Moreover, for the fundamental harmonic there is no clear trend in the reactive power correlated to the decrease of the PBMIF in Fig. 12b. In contrast, the third harmonic component of the reactive power shows a monotonic increase for increasing forcing level but the overall level of the third harmonic of the reactive power is with less than 5% of the active power still comparably small. The evaluation of the relative distortion power D/S in Fig. 13b shows that this power quantity also increases with increasing excitation level (or frequency respectively). This increase of the distortion power indicates that for higher

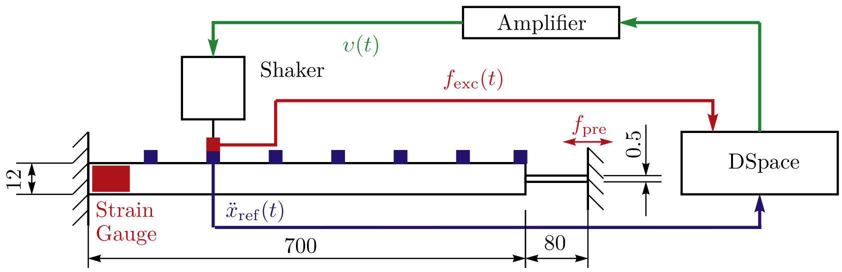

Fig. 10. Schematic sketch of the experimental setup.

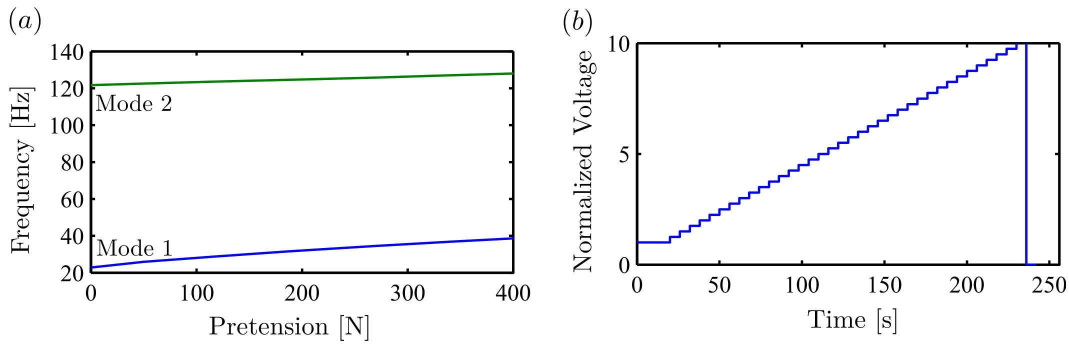

Fig. 11. (a): Eigenfrequencies of mode 1 and 2 depending on pretension. (b): Normalized shaker input voltage over time for PLL test.

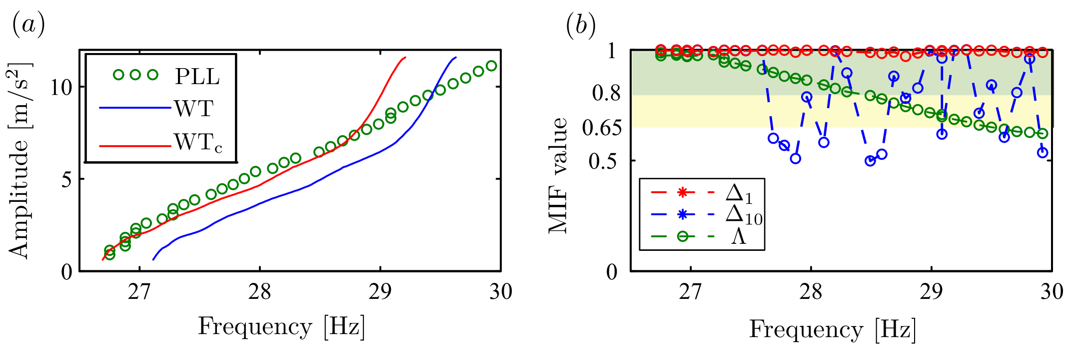

Fig. 12. (a): Measured backbone with PLL method, WT of free-decay and corrected WT of free-decay. (b): Fundamental harmonic MPI Δ_1, higher harmonic MPI Δ_{10} and PBMIF Λ.

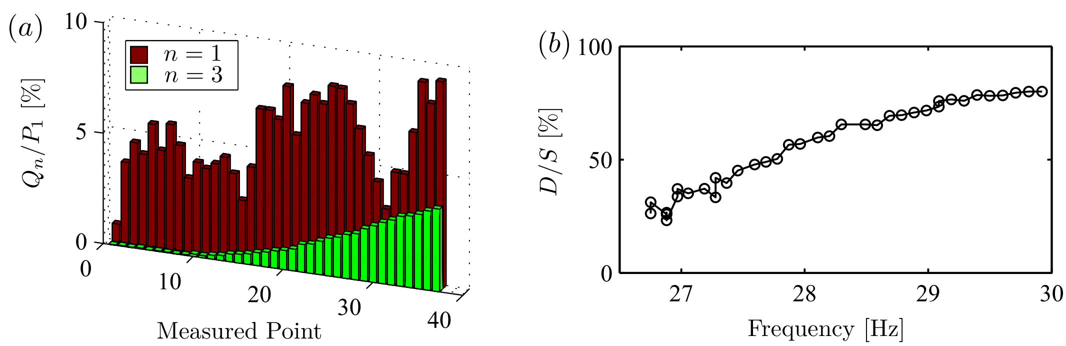

Fig. 13. (a): Relative reactive power of first, third and fifth harmonic component of the excitation. (b): Distortion power over frequency.

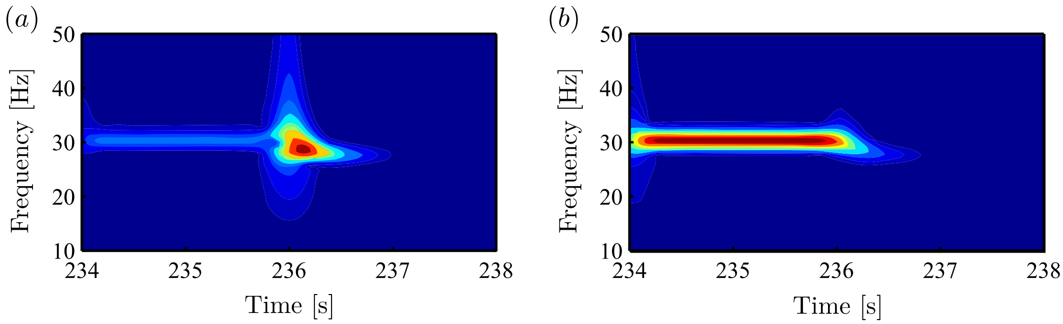

Fig. 14. (a): WT of the force signal at node 2. at the instant of switching off the shaker. (b): WT of the acceleration signal at node 2. at the instant of switching off the shaker.

forcing levels there is increasing power transfer to higher harmonics and other DOFs. Indeed the influence of the relative distortion power on the value of the PBMIF is, in this case, much higher than the influence of the reactive power Q. For an improvement of the NNM appropriation quality therefore the power considerations indicate that the phase (to decrease the relative reactive power of the third harmonic) and amplitude (to decrease the distortion power) of higher harmonics, in this case mostly the third harmonic, need to be controlled. Additionally, the location and spatial distribution of the forcing can be changed in order to reduce the relative distortion power. Nevertheless, the test also shows that the PLL method is generally capable of tracking the first order backbone curve with the same accuracy as the previous methods that used single harmonic, single point forces [27,10]. The method provides steady-state measurements within a very short measurement time for which the force appropriation quality of the NNMs can be easily evaluated by the PBMIF. For comparison the results obtained by free-decay testing are shown in Section 6.1.

6.1. Comparison to free-decay test

The results obtained by the PLL method are also compared to the free-decay method which is most commonly used for nonlinear phase resonance testing. To this end, the shaker was switched off after the PLL measurement at a measurement time of 236 s. At this time an imperfect single harmonic force appropriation is reached by the PLL excitation, as it was previously done by manual tuning of the excitation frequency. After the shaker is switched off, the free-decay is recorded. The time history of the free-decay is analyzed using a Morlet WT to obtain the time-frequency dependence and the ridge of the WT is reconstructed to recover the time amplitude dependence. For details regarding the implementation of the WT and the ridge reconstruction used in this paper the reader is referred to [40,15]. The ridge of the WT is displayed in Fig. 12a as blue curve. Compared to the PLL test, two major differences are evident: Firstly, there is a deviation for high amplitudes and, secondly, there is a shift in frequency which seems to be constant over the amplitude range from 0 to 7 $\mathrm{m/s^2}$.

The first difference can be explained by analyzing the force signal when the shaker is switched off. Therefore, a WT is applied to the recorded force signal (see. Fig. 14a). At the instant when the shaker is switched off (236 s) a significant impulsive force is induced which also increases the instantaneous forcing frequency for a short time. This impulsive force also disturbs the response such that the frequency amplitude dependence is biased at the time when the shaker is switched off. It is interesting to note that the impulsive force, which is obvious in the force signal, is hardly visible in the WT acceleration signal (see Fig. 14b). This can also be one explanation that after the initial perturbation dies out the course of the backbone curve obtained by the free-decay of the acceleration resembles the one obtained with the PLL method. This observation also matches previous experimental studies that found the influence of the shaker on the free-decay response to be small [22]. Nevertheless, there is still a significant force measured in the load cell at the excitation point during the whole decay process. This force is induced by the inertia of the shaker and the stiffness of the stinger attached to the structure. The influence of these attachments was assessed experimentally by two sets of linear EMAs: One EMA with active shaker (low level random shaker exciation) and one EMA with passive shaker attached to the structure (low level impact hammer exciation). The difference of the eigenfrequencies for both tests can directly be attributed to the influence of the passive shaker as for the first test the input for the EMA is measured directly at the excitation point on the structure, i.e. the reaction force between shaker and structure. Thus the influence of the shaker and stinger is eliminated. In contrast, for the second test the input force is measured with the load cell of an impact hammer independently of the shaker structure interaction, such that the modes of the structure including the stinger and passive shaker are obtained. The first eigenfrequency with the passive shaker attachment was found to be 0.42 Hz higher than the eigenfrequency of the structure with the active shaker. If one assumes that this influence is approximately linear (i.e. independent of amplitude), then one can shift the backbone curve of the free-decay results with passive shaker depicted in Fig. 12a (blue curve) by 0.42 Hz yielding the red curve corresponding to the free-decay of the structure without influence of the passive shaker. The obtained curve shows an excellent agreement with the PLL results after the initial disturbance dies out. Thus, on the one hand this shows that the results of the new method are comparable to the results obtained with free-decay measurements. On the other hand this helps to evaluate the quality of the previously used free-decay measurements, as for the steady-state results obtained with PLL excitation the quality of the NNM approximation can actually be evaluated with the PBMIF. A comparison of both results therefore helps to understand the accuracy and limitations of the free-decay method. For the present experimental example the influence of the shaker was found to be non-negligible in free-decay measurements but it could be minimized by additional consideration of the shaker dynamics. Of course, the results of the free-decay method can also be improved by non-contact excitation techniques.

7. Conclusion

This paper proposes a novel framework for nonlinear phase resonance testing that relies on excitation power considerations in conjunction with steady-state phase control measurements. It is shown that the mechanical power of the excitation is a central quantity by means of NNM isolation. Therefore, power definitions well-known from nonlinear electrical systems are transferred to nonlinear structural dynamics applications. The new definitions are fully consistent with power considerations known from linear phase resonance testing. The fundamental difference caused by the limited physical meaning of the reactive power in nonlinear situations is emphasized. The apparent power provides a more meaningful quantity in the nonlinear case and has a high relevance in nonlinear phase resonance testing. On this foundation a new type of mode indicator function for nonlinear modal testing, the PBMIF, is defined. This mode indicator is easy to implement, robust and reliable.

For the evaluation of the excitation power quantities the backbone curve has to be measured in terms of a series of steady-state measurements. To circumvent the issues related to manual tuning of the excitation frequency an automated controller is implemented. For this purpose the PLL concept is used which provides a very fast and robust method of generating and adjusting the excitation signal based on its phase with respect to a reference signal. With this controller the advantages of in terms of robustness of phase control over traditional frequency-controlled measurements can be exploited. Using the PBMIF the confidence of every measured point on the backbone curve can be directly evaluated.

Both, the PBMIF and the PLL excitation are shown to be user-friendly methods also in experimental situations. The experimental demonstration on a benchmark beam structure exhibiting stiffening behavior shows the robustness and speed of the PLL controller for nonlinear phase resonance testing. The PBMIF clearly indicates the confidence of the isolated NNMs, also in the presence of higher harmonics, and additional power considerations help to locate possible sources of inaccuracies. The comparison to the previously used free-decay method shows an excellent agreement. Even more importantly, the confidence of the free-decay tests can be evaluated on the basis of the PLL tests. In this paper the free-decay tests are obtained by simply switching off the shaker and it is shown that the influence of the passive shaker attached to the structure is twofold: At the instant of switching off the excitation an impulsive force is induced on the structure and the passive shaker shifts the eigenfrequencies by its additional mass and stiffness properties. Whereas the former effect is difficult to quantify the latter can easily be identified quantitatively by simple linear EMAs. Nonetheless, the analysis shows that the influence of the shaker in free-decay measurements is generally non-negligible such that this type of measurements should be handled with care.

References

[1] G. Kerschen, K. Worden, A.F. Vakakis, J.-C. Golinval, Past, present and future of nonlinear system identification in structural dynamics, Mech. Syst. Sign. Process. 20 (April) (2006) 505–592.
[2] K. Worden, G.R. Tomlinson, Nonlinearity in Structural Dynamics, Institute of Physics Publishing, Bristol, 2001.
[3] B.F. Feeny, R. Kappagantu, On the physical interpretation of proper orthogonal modes in vibrations, J. Sound Vib. 211 (1998) 607–616.
[4] G. Kerschen, M. Peeters, J.C. Golinval, A.F. Vakakis, Nonlinear normal modes, Part I: A useful framework for the structural dynamicist, Mech. Syst. Sign. Process. 23 (January) (2009) 170–194.
[5] R.M. Rosenberg, Normal modes of nonlinear dual-mode systems, J. Appl. Mech. 27 (2) (1960) 263–268.
[6] S.W. Shaw, C. Pierre, Normal modes for non-linear vibratory systems, J. Sound Vib. 164 (1) (1992) 85–124.
[7] M. Peeters, R. Viguié, G. Sérandour, G. Kerschen, J.C. Golinval, Nonlinear normal modes, Part II: Toward a practical computation using numerical continuation techniques, Mech. Syst. Sign. Process. 23 (January) (2009) 195–216.
[8] W. Szemplinska-Stupnicka, The modified single mode method in the investigations of the resonant vibration of non-linear systems, J. Sound Vib. 63 (4) (1979) 475–489.
[9] D.J. Ewins, Modal Testing: Theory, Practice and Application, second ed., Research Studies Press Ltd., Baldock, 2000.
[10] M. Peeters, G. Kerschen, J.C. Golinval, Modal testing using nonlinear normal modes: an experimental demonstration, in: Proceedings of ISMA, (Leuven, Belgium), 2010, pp. 3221–3236.
[11] Jean-Philippe Noël, L. Renson, C. Grappasonni, G. Kerschen, Identification of nonlinear normal modes of engineering structures under broadband forcing, Mech. Syst. Sign. Process. 74 (2016) 95–110.
[12] S. Peter, A. Grundler, P. Reuss, L. Gaul, R.I. Leine, Towards finite element model updating based on nonlinear normal modes, in: G. Kerschen (Ed.), Nonlinear Dynamics, Proceedings of the 33rd IMAC, A Conference and Exposition on Structural Dynamics 2015, vol. 1, Springer, 2016, pp. 209–217.
[13] J.L. Zapico-Valle, M. García-Diéguez, R. Alonso-Camblor, Nonlinear modal identification of a steel frame, Eng. Struct. 56 (2013) 246–259.
[14] J.M. Londono, S.A. Neild, J.E. Cooper, Identification of backbone curves of nonlinear systems from resonance decay responses, J. Sound Vib. 348 (2015) 224–238.
[15] W.J. Staszewski, Identification of damping in MDOF systems using time-scale decomposition, J. Sound Vib. 203 (2) (1997) 283–305.
[16] M. Feldman, Non-linear system vibration analysis using Hilbert transform – I. Free vibration analysis method 'freevib', Mech. Syst. Sign. Process. 8 (2) (1994) 119–127.
[17] R.J. Kuether, M.R.W. Brake, Instantaneous frequency and damping from transient ring-down data, in: M.S. Allen, R.L. Mayes, D. Rixen (Eds.), Dynamics of Coupled Structures, Proceedings of the 34th IMAC, A Conference and Exposition on Structural Dynamics 2016, vol. 4, Springer, Bethel, 2016, pp. 253–263.
[18] D.A. Ehrhardt, M.S. Allen, Measurement of nonlinear normal modes using multi-harmonic stepped force appropriation and free decay, Mech. Syst. Sign. Process. 76–77 (2016) 612–633.
[19] J.R. Wright, J.E. Cooper, M.J. Desforges, Normal-mode force appropriation – theory and application, Mech. Syst. Sign. Process. 13 (2) (1999) 217–240.
[20] M. Géradin, D.J. Rixen, Mechanical Vibrations: Theory and Application to Structural Dynamics, third ed., Wiley, Chichester, 2015.

[21] R. Gasch, K. Knothe, R. Liebich, Struktu rdyna mik, second ed., Springer-Verlag, Heidelberg, 2012.
[22] M. Peeters, G. Kerschen, J.C. Golinval, Dynamic testing of nonlinear vibrating structures using nonlinear normal modes, J. Sound Vib. 330 (January) (2011) 486–509.
[23] R.J. Kuether, L. Renson, T. Detroux, C. Grappasonni, G. Kerschen, M.S. Allen, Nonlinear normal modes, modal interactions and isolated resonance curves, J. Sound Vib. 351 (2015) 299–310.
[24] C. Budeanu, Puissances réactives et fictives, Impr. Cultura Nationala, Bucharest, 1927.
[25] S. Svensson, Power Measurement Techniques for Non-sinusoidal Conditions Dissertation, Chalmers University of Technology, 1999.
[26] L.S. Czarnecki, What is wrong with the Budeanu concept of reactive and distortion power and why it should be abandoned, IEEE Trans. Instrum. Meas. IM-36 (3) (1987) 834–837.
[27] L. Renson, A. Gonzalez-Buelga, D. Barton, S. Neild, Robust identification of backbone curves using control-based continuation, J. Sound Vib. 367 (2016) 145–158.
[28] D. Abramovitch, Phase-locked loops: a control centric tutorial, Proceedings of the 2002 American Control Conference (IEEE Cat. No. CH37301, vol. 1, 2002, pp. 1–15.
[29] G.-C. Hsieh, J.C. Hung, Phase-locked loop techniques – a survey, IEEE Trans. Ind. Electron. 43 (6) (1996) 609–615.
[30] X. Sun, R. Horowitz, K. Komvopoulos, Stability and resolution analysis of a phase-locked loop natural frequency tracking system for MEMS fatigue testing, J. Dyn. Syst. Meas. Contr. Trans. ASME 124 (4) (2002) 599–605.
[31] M. Fan, M. Clark, Z. Feng, Implementation and stability study of phase-locked-loop nonlinear dynamic measurement systems, Commun. Nonlinear Sci. Numer. Simul. 12 (October) (2007) 1302–1315.
[32] I. Sokolov, V. Babitsky, Phase control of self-sustained vibration, J. Sound Vib. 248 (4) (2001) 725–744.
[33] S. Mojrzisch, I. Ille, J. Wallaschek, Phase controlled frequency response measurement for nonlinear vibration systems, in: Proceedings of ICSV, (Bangkok, Thailand), 2013.
[34] R. García, R. Pérez, Dynamic atomic force microscopy methods, Surf. Sci. Rep. 47 (2002) 197–301.
[35] V.I. Babitsky, I.J. Sokolov, Autoresonant homeostat concept for engineering application of nonlinear vibration modes, Nonlinear Dyn. 50 (3) (2007) 447–460.
[36] S. Peter, F. Schreyer, P. Reuss, L. Gaul, Consideration of local stiffening and clearance nonlinearities in coupled systems using a generalized Harmonic balance method, in: Proceedings of the International Conference on Noise and Vbration Engineering ISMA 2014, (Leuven, Belgium), 2014.
[37] F. Thouverez, Presentation of the ECL benchmark, Mech. Syst. Sign. Process. 17 (January) (2003) 195–202.
[38] S. Meyer, Modellbildung und Identifikation von lokalen Steifigkeits- und Dämpfungseigenschaften in komplexen strukturdynamischen Finite Elemente Modellen Dissertation, Kassel University, 2003.
[39] A.D. Shaw, T.L. Hill, S.A. Neild, M.I. Friswell, Experimental identification of a structure with internal resonance, in: G. Kerschen (Ed.), Nonlinear Dynamics, Proceedings of the 34th IMAC, A Conference and Exposition on Structural Dynamics 2016, vol. 1, Springer, Bethel, 2016, pp. 37–45.
[40] D. Jordan, R.W. Miksad, E.J. Powers, Implementation of the continuous wavelet transform for digital time series analysis, Rev. Sci. Instrum. 68 (3) (1997) 1484.